

Communication

# On the Importance of Halogen Bonding Interactions in Two X-ray Structures Containing All Four (F, Cl, Br, I) Halogen Atoms

Dmitriy F. Mertsalov <sup>1</sup>, Rosa M. Gomila <sup>2</sup>, Vladimir P. Zaytsev <sup>1</sup>, Mikhail S. Grigoriev <sup>3</sup>, Eugeniya V. Nikitina <sup>1</sup>, Fedor I. Zubkov <sup>1,\*</sup> and Antonio Frontera <sup>2,\*</sup>

<sup>1</sup> Faculty of Science, Peoples' Friendship University of Russia (RUDN University), 6 Miklukho-Maklaya St., 117198 Moscow, Russia; keithred@mail.ru (D.F.M.); vzaitsev@sci.pfu.edu.ru (V.P.Z.); enikitina@sci.pfu.edu.ru (E.V.N.)

<sup>2</sup> Department of Chemistry, Universitat de les Illes Balears, Crta. de Valldemossa km 7.5, 07122 Palma, Spain; rosa.gomila@uib.es

<sup>3</sup> Frumkin Institute of Physical Chemistry and Electrochemistry, Russian Academy of Sciences, 31/4 Leninskiy prosp., 119071 Moscow, Russia; mickgrig@mail.ru

\* Correspondence: fzubkov@sci.pfu.edu.ru (F.I.Z.); toni.frontera@uib.es (A.F.)

**Abstract:** This manuscript reports the synthesis and X-ray characterization of two octahydro-1H-4,6-epoxycyclopenta[c]pyridin-1-one derivatives that contain the four most abundant halogen atoms (Ha) in the structure with the aim of studying the formation of Ha...Ha halogen bonding interactions. The anisotropy of electron density at the heavier halogen atoms provokes the formation of multiple Ha...Ha contacts in the solid state. That is, the heavier Ha-atoms exhibit a region of positive electrostatic potential ( $\sigma$ -hole) along the C–Ha bond and a belt of negative electrostatic potential ( $\sigma$ -lumps) around the atoms. The halogen bonding assemblies in both compounds were analyzed using density functional theory (DFT) calculations, molecular electrostatic potential (MEP) surfaces, the quantum theory of “atom-in-molecules” (QTAIM), the noncovalent interaction plot (NCIplot), and the electron localization function (ELF).

**Keywords:** halogen bonding; crystal engineering; supramolecular chemistry;  $\sigma$ -hole



**Citation:** Mertsalov, D.F.; Gomila, R.M.; Zaytsev, V.P.; Grigoriev, M.S.; Nikitina, E.V.; Zubkov, F.I.; Frontera, A. On the Importance of Halogen Bonding Interactions in Two X-ray Structures Containing All Four (F, Cl, Br, I) Halogen Atoms. *Crystals* **2021**, *11*, 1406. <https://doi.org/10.3390/cryst11111406>

Academic Editors: Sergiy Rosokha and Atash V. Gurbanov

Received: 31 October 2021

Accepted: 16 November 2021

Published: 18 November 2021

**Publisher's Note:** MDPI stays neutral with regard to jurisdictional claims in published maps and institutional affiliations.



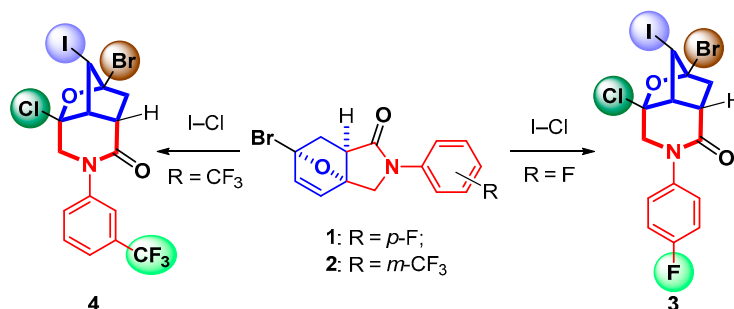
**Copyright:** © 2021 by the authors. Licensee MDPI, Basel, Switzerland. This article is an open access article distributed under the terms and conditions of the Creative Commons Attribution (CC BY) license (<https://creativecommons.org/licenses/by/4.0/>).

## 1. Introduction

A profound comprehension of noncovalent interactions is needed to succeed in the competitive field of supramolecular chemistry [1]. For instance, construction of precise hosts is key in supramolecular catalysis [2,3] for activating the substrate and lowering the barrier of the transition state. Compared to the ubiquitous nature of hydrogen bonding (HB) [4], halogen bonding (HaB) is attracting substantial interest by the research community [5–8] due to its high directionality and tunability, thus proved valuable in catalysis, pharmacology, and material science [6–10]. Therefore, the preparation and solid state characterization of halogenated compounds is of interest to further understand the behavior and directing role of HaBs.

The Wagner–Meerwein rearrangement is a well-known synthetic transformation in which a group (or H-atom) migrates from one carbon to a neighboring carbon [11,12], promoted by Lewis [13] or a Brønsted acids [14]. Moreover, several works have also used halogenation to initiate Wagner–Meerwein rearrangements [15–17]. It should be mentioned that the halogen-initiated cationic rearrangement in 7-oxabicycloheptenes, condensed with other heterocycles, was first demonstrated in 1985 [18]. Later, it was shown that *N*-bromosuccinimide (NBS) or bromine and iodine or ICl are the best reagents for halogen-promoted skeletal rearrangements in bridge systems such as 4a,7-epoxyisoquinolines, 3a,6-epoxyisoindoles, and 4,6-epoxycyclopenta[c]pyridines [17,19–21].

Inspired by the last work [17], where three halogen atoms (Cl, Br, and I) were incorporated in the aliphatic skeleton of the target molecule, we envisaged the synthesis and X-ray characterization of 4,5,6-trihalo-2-aryl-4,6-epoxycyclopenta[*c*]pyridin-1-ones (**3** and **4**) starting from the rearrangement of 3a,6-epoxyisoindoles **1** and **2** under the action of ICl (Scheme 1). Iodine monochloride was chosen as a reactant due to its rather rare use in organic chemistry and its ability to provide a product with two different halogen atoms at once.



**Scheme 1.** Synthesis of halogenated compounds **3** and **4** using halogenation-mediated Wagner–Meerwein rearrangement reaction.

Comprising in their structure at once the four halogen atoms (F, Cl, Br, and I), halides **3** and **4** were considered to be ideal models for analyzing the competition between different halogens to participate in halogen and hydrogen bonding interactions. In addition, note that not a long list of organic molecules containing simultaneously all four halogen atoms in their skeleton can be found in the literature [22–24]. In particular, Shellhamer et al. opened a short passway to polyhalogenated alkanes through the rearrangement of five-membered halonium ions, generated from terminal alkenes under action of chlorine, bromine, iodine monobromide, and iodine monochloride [22,23]. In 2006, another outstanding work [24] made available for further study polyhalocubanes with a wide assortment of different halogens in the apical positions.

The solid-state architectures of both compounds **3** and **4** reveal the existence of numerous Ha···Ha contacts, which have been characterized by means of several computational tools, including MEP, QTAIM, NCIPLOT, and ELF. Moreover, the energetic features of some dimers have been evaluated using DFT calculations, as detailed in the next sections.

## 2. Materials and Methods

### 2.1. Synthesis and Spectral Characteristics of Compounds **3** and **4** (General Method)

The solution of the corresponding isoindolone **1** or **2** (0.62 mmol) and iodine monochloride (0.62 mmol) in 3 mL of dry dichloromethane was stirred for 3 d (for **3**) or 2 d (for **4**) at r.t (TLC control, EtOAc–hexane, 1:2, Sorbfil). The reaction mixture was poured into H<sub>2</sub>O (50 mL) and extracted with CH<sub>2</sub>Cl<sub>2</sub> (3 × 20 mL). The combined organic fractions were washed with saturated solution Na<sub>2</sub>S<sub>2</sub>O<sub>3</sub> (20 mL) and dried over anhydrous Na<sub>2</sub>SO<sub>4</sub>. The solvent was evaporated under reduced pressure, and the residue was recrystallized from a hexane–AcOEt mixture.

**(4*SR*,4*aRS*,5*SR*,6*SR*,7*aSR*)-6-Bromo-4-chloro-2-(4-fluorophenyl)-5-iodooctahydro-1*H*-4,6-epoxycyclopenta[*c*]pyridin-1-one (**3**).** Yield 70%, m.p. 211–212 °C (decomposition), light beige prisms, <sup>1</sup>H NMR (600.2 MHz, DMSO-*d*<sub>6</sub>) δ 7.37 (dd, *J*~9.1 Hz, *J*~5.0 Hz, 2H, H-3, H-5 H<sub>arom.</sub>), 7.23 (t, *J*~9.1 Hz, 2H, H-2, H-6 H<sub>arom.</sub>), 4.92 (s, 1H, H-5), 4.36 (d, *J*~13.1 Hz, 1H), 4.02 (d, *J*~13.1 Hz, 1H, H-3), 3.57 (dd, *J*~4.5 Hz, *J*~1.0 Hz, 1H, H-4a), 3.17 (dt, *J*~4.2 Hz, *J*~11.6 Hz, 1H, H-7a), 2.81 (dd, *J*~11.6 Hz, *J*~12.9 Hz, 1H, H-7<sub>exo</sub>), 1.76 (dd, *J*~4.2 Hz, *J*~12.9 Hz, 1H, H-7<sub>endo</sub>). <sup>13</sup>C NMR (150.9 MHz, DMSO-*d*<sub>6</sub>) δ 168.9, 160.5 (d, *J*~244.2 Hz), 137.0 (d, *J*~2.9 Hz), 128.3 (d, *J*~8.7 Hz, 2C), 115.6 (d, *J*~23.1 Hz, 2C), 102.9, 96.3, 58.6, 49.6, 44.2, 41.1, 29.2. <sup>19</sup>F NMR (564.7 MHz, DMSO-*d*<sub>6</sub>) δ −115.0. IR (KBr): 1670 (NC=O), 1089 (C-F), 619 (C-Br). MS (ESI): *m/z* = 486 [M+H<sup>+</sup>] (<sup>35</sup>Cl,<sup>79</sup>Br), 488 [M+H<sup>+</sup>] (<sup>37</sup>Cl,<sup>79</sup>Br), 490 [M + H<sup>+</sup>]

( $^{37}\text{Cl}$ ,  $^{81}\text{Br}$ ). Anal. Calcd for  $\text{C}_{14}\text{H}_{11}\text{BrClFINO}_2$ : C, 34.56; H, 2.28; N, 2.88. Found: C, 34.50; H, 2.23; N, 2.96.

**(4SR,4aRS,5SR,6RS,7aSR)-6-Bromo-4-chloro-5-iodo-2-[3-(trifluoromethyl)phenyl]octahydro-1H-4,6-epoxycyclopenta[c]pyridin-1-one (4)**. Yield 45%, m.p. 210–211 °C (decomposition), colorless thin needles.  $^1\text{H}$  NMR (600.2 MHz,  $\text{CDCl}_3$ )  $\delta$  7.61–7.56 (m, 2H, H-4, H-5, H-2  $\text{H}_{\text{arom.}}$ ), 7.53 (s, 1H, H-2  $\text{H}_{\text{arom.}}$ ), 7.46 (d,  $J \sim 7.6$  Hz, 1H, H-6  $\text{H}_{\text{arom.}}$ ), 4.48 (s, 1H, H-5), 4.28 (d,  $J \sim 13.8$  Hz, 1H), 4.24 (d,  $J \sim 13.8$  Hz, 1H, H-3), 3.37 (dd,  $J \sim 4.2$  Hz,  $J \sim 1.0$  Hz, 1H, H-4a), 3.26 (dt,  $J \sim 4.2$  Hz,  $J \sim 11.3$  Hz, 1H, H-7a), 2.85 (dd,  $J \sim 11.3$  Hz,  $J \sim 13.1$  Hz, 1H, H-7exo), 2.42 (dd,  $J \sim 4.2$  Hz,  $J \sim 13.1$  Hz, 1H, H-7endo).  $^{13}\text{C}$  NMR (150.9 MHz,  $\text{CDCl}_3$ )  $\delta$  168.6, 140.4, 132.1 (q,  $J \sim 33.2$  Hz), 130.1, 129.3, 124.5 (q,  $J \sim 4.3$  Hz), 122.7 (q,  $J \sim 4.3$  Hz), 123.4 (q,  $J \sim 272.3$  Hz), 100.5, 94.9, 59.5, 50.0, 45.3, 41.7, 28.0.  $^{19}\text{F}$  NMR (564.7 MHz,  $\text{CDCl}_3$ )  $\delta$  –62.5. IR (KBr): 1664 (NC=O), 1337, 1130 (C-F), 729 (C-Cl), 637 (C-Br). MS (ESI):  $m/z = 536$  [ $\text{M}+\text{H}^+$ ] ( $^{35}\text{Cl}$ ,  $^{79}\text{Br}$ ), 538 [ $\text{M} + \text{H}^+$ ] ( $^{37}\text{Cl}$ ,  $^{79}\text{Br}$ ), 540 [ $\text{M}+\text{H}^+$ ] ( $^{37}\text{Cl}$ ,  $^{81}\text{Br}$ ). Anal. Calcd for  $\text{C}_{15}\text{H}_{11}\text{BrClF}_3\text{INO}_2$ : C, 33.58; H, 2.07; N, 2.61. Found: C, 33.52; H, 2.01; N, 2.73.

## 2.2. XRD Experimental Part

The X-ray diffraction data were collected on a Bruker Kappa Apex II automatic four-circle diffractometer (Bruker AXS Inc., Madison, WI, USA) equipped with an area detector (Mo-K $\alpha$  sealed-tube X-ray source,  $\lambda = 0.71073$  Å, graphite monochromator) at 100 K for all compounds.

The data frames were collected using the program APEX2 and processed using the program SAINT routine within APEX2. The unit cell parameters were refined over the whole dataset [25]. The data were corrected for absorption on the multi-scan technique as implemented in SADABS [26]. The structures were solved by direct methods using SHELXS and refined by full-matrix least-squares on  $F^2$  using SHELXL-2018/3 software [27] in the anisotropic approximation for all non-hydrogen atoms. Hydrogen atoms on carbon were calculated in ideal positions with isotropic displacement parameters set to  $1.2 \times U_{\text{eq}}(\text{C})$ . The structure 3 was refined as an inversion twin with the contribution of the second domain 0.436(12). Tables and pictures for structures were generated using Olex2 as GUI [28]. Crystallographic data and structural refinements details are summarized in Table 1.

**Table 1.** Crystal data and structure refinement for 3 and 4.

Compound	3	4
CCDC number	2118649	2118650
Empirical formula	$\text{C}_{14}\text{H}_{11}\text{NO}_2\text{FCIBrI}$	$\text{C}_{15}\text{H}_{11}\text{NO}_2\text{F}_3\text{ClIBrI}$
Formula weight	486.50	536.51
Temperature/K	100(2)	100(2)
Crystal system	orthorhombic	monoclinic
Space group	$Pca2_1$	$P2_1/c$
a/Å	19.310(2)	12.2575(9)
b/Å	7.2206(8)	7.0718(5)
c/Å	22.530(3)	19.2040(13)
$\alpha/^\circ$	90	90
$\beta/^\circ$	90	90.781(4)
$\gamma/^\circ$	90	90
Volume/Å <sup>3</sup>	3141.4(6)	1664.5(2)
Z	8	4

Table 1. Cont.

Compound	3	4
$\rho_{\text{calc}}/\text{cm}^3$	2.057	2.141
$\mu/\text{mm}^{-1}$	4.765	4.524
$F(000)$	1856.0	1024.0
Crystal size/ $\text{mm}^3$	$0.16 \times 0.12 \times 0.08$	$0.4 \times 0.18 \times 0.14$
Radiation	MoK $\alpha$ ( $\lambda = 0.71073$ )	MoK $\alpha$ ( $\lambda = 0.71073$ )
2 $\Theta$ range for data collection/ $^\circ$	8.378 to 54.998	6.968 to 70
Index ranges	$-25 \leq h \leq 25$ , $-9 \leq k \leq 8$ , $-29 \leq l \leq 29$	$-19 \leq h \leq 19$ , $-11 \leq k \leq 10$ , $-30 \leq l \leq 30$
Reflections collected	44,518	42,785
Independent reflections	7191 [ $R_{\text{int}} = 0.0816$ , $R_{\text{sigma}} = 0.0605$ ]	7322 [ $R_{\text{int}} = 0.0282$ , $R_{\text{sigma}} = 0.0217$ ]
Data/restraints/parameters	7191/1/380	7322/0/245
Goodness-of-fit on $F^2$	1.016	1.030
Final $R$ indexes [ $I \geq 2\sigma(I)$ ]	$R_1 = 0.0344$ , $wR_2 = 0.0575$	$R_1 = 0.0216$ , $wR_2 = 0.0443$
Final $R$ indexes [all data]	$R_1 = 0.0503$ , $wR_2 = 0.0617$	$R_1 = 0.0310$ , $wR_2 = 0.0468$
Largest diff. peak/hole/ $e \text{ \AA}^{-3}$	0.93/−0.67	0.57/−1.00

X-ray diffraction experiments were performed at the Center for Shared Use of Physical Methods of Investigation at the Frumkin Institute of Physical Chemistry and Electrochemistry, RAS (CKP FMI IPCE RAS). Atomic coordinates for compounds **3** and **4** have been deposited with the Cambridge Crystallographic Data Centre (CCDC numbers are 2118649 for **3** and 2118650 for **4**). The supplementary crystallographic data can be obtained free of charge from the Cambridge Crystallographic Data Centre via [www.ccdc.cam.ac.uk/data\\_request/cif](http://www.ccdc.cam.ac.uk/data_request/cif) (accessed on 17 November 2021).

### 2.3. Computational Details

The calculations reported herein were performed using the Turbomole 7.2 program [29]. The crystallographic coordinates were used for the calculations of the supramolecular assemblies. For the MEP surface calculations, fully optimized geometries were used. We used the crystallographic coordinates for the assemblies because we are interested in evaluating the interactions as they stand in the solid state. The purpose of this manuscript is not finding the most favorable orientation of the molecules in the isolated assemblies (dimers, trimers, and tetramers) in the gas phase. The level of theory used for the calculations was PB86-D3/def2-TZVP [30–32]. For iodine, this basis set includes effective core potentials (ECP) and takes into consideration relativistic effects for the inner electrons [32]. This level of theory has been used before to evaluate noncovalent interactions in the solid state [33,34]. The MEP surface plots were generated using the wavefunction obtained at the same level of theory and the 0.01 a.u. isosurface to simulate the van der Waals envelope. The topological analysis of the electron density was carried out according to the quantum theory of atoms in molecules (QTAIM) and noncovalent interaction plot index (NCIplot) methods proposed by Bader [35] and W. Yang et al. [36], respectively. Both were represented using the VMD program [37] and using the following settings for the NCIplot index representation:  $s = 0.5$  a.u.; cut-off  $\rho = 0.04$  a.u., and color scale  $-0.04 \leq \text{sign}(\lambda_2)\rho \leq 0.04$  a.u. The electron localization function (ELF) [38] analysis was performed using the MultiWFN program [39] at the PB86-D3/def2-TZVP level of theory.

### 3. Results and Discussion

#### 3.1. Structural Description of Compounds 3 and 4

Molecular structures of compounds **3** and **4** are shown in Figures S3 and S4 (Tables S1–S13) and their brief description are given below.

The structure **3** contains two crystallographically independent formula units. Both independent molecules have the same conformation (root-mean-square deviation for atoms of the superimposed molecules is 0.045 Å). The CF<sub>3</sub> group in **4** is disordered. Selected bond lengths for the structures **3** and **4** are given in Table 2. For all the three molecules, corresponding distances are practically the same. A difference can be seen only for the conformation of **4** as compared with two molecules in **3**; the phenyl ring is rotated by about 10° (see Tables S5 and S10). Crystal packing for both compounds can be described as layers of molecules with alternating orientation (Figures S5 and S6).

**Table 2.** Selected bond lengths in the structures **3** and **4**.

Bond	Length/Å	Length/Å	Length/Å
	<b>3</b> , molecule <b>A</b>	<b>3</b> , molecule <b>B</b>	<b>4</b>
I1-C5	2.146(8)	2.138(7)	2.1361(12)
Br1-C6	1.922(7)	1.913(7)	1.9150(12)
Cl1-C4	1.815(7)	1.814(8)	1.8202(12)
O1-C1	1.236(9)	1.224(9)	1.2262(16)
O8-C4	1.420(9)	1.416(9)	1.4177(15)
O8-C6	1.453(8)	1.446(8)	1.4457(16)
N2-C1	1.354(9)	1.364(10)	1.3576(17)
N2-C3	1.465(9)	1.461(9)	1.4621(16)
N2-C11	1.437(9)	1.446(9)	1.4369(17)
C1-C7A	1.501(10)	1.526(10)	1.5111(18)
C3-C4	1.523(10)	1.492(10)	1.5159(18)
C4-C4A	1.506(10)	1.518(10)	1.5189(18)
C4A-C5	1.534(10)	1.535(10)	1.5394(18)
C4A-C7A	1.573(10)	1.560(10)	1.5612(18)
C5-C6	1.523(10)	1.526(10)	1.5261(18)
C6-C7	1.506(10)	1.531(10)	1.5219(18)
C7-C7A	1.585(11)	1.567(11)	1.5755(18)

#### 3.2. DFT Calculations

First, the MEP surface of compound **3** was computed and represented in Figure 1 to investigate the most electron rich and electron poor region of the molecule. Moreover, it is also convenient to examine the size and intensity of the  $\sigma$ -holes. It can be observed that the MEP minimum is located at the O-atom of the amido group (−34.9 kcal/mol) and the maximum at the CH groups of the cyclopentanyl rings (+30.9 kcal/mol, see Figure 1). Details of the MEP surface around the four halogen atoms are also included in Figure 1 where a reduced MEP scale was used ( $\pm 18$  kcal/mol). As expected, the heaviest halogen atom presents the largest and more intense  $\sigma$ -hole (+18.1 kcal/mol) followed by the bromine (+13.9 kcal/mol) thus anticipating a large ability to establish halogen bonding interactions. In contrast, the chlorine atom shows a very small and positive MEP value opposite to the C–Cl bond (+3.0 kcal/mol), therefore much lower propensity to participate in  $\sigma$ -hole interactions. Finally, the MEP value for fluorine is negative, thus adequate to establish HBs or HaBs as acceptors.

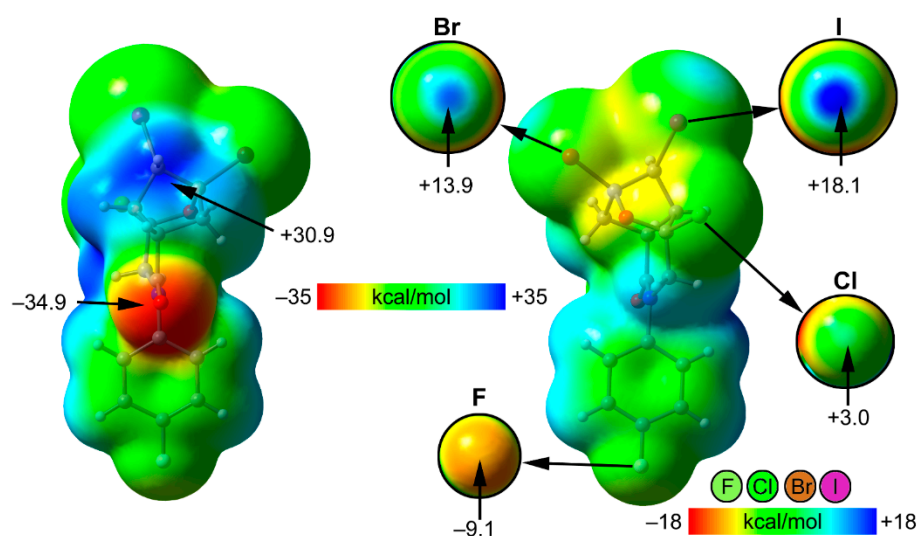


**Figure 1.** Two views of the MEP surface of optimized compound **3** at the PB86-D3/def2-TZVP level of theory. Details of the MEP around the halogen atoms is also indicated (encircled regions) where a reduced  $\pm 18$  kcal/mol energy range has been used. The energies at selected points of the surface are given in kcal/mol.

The energetic DFT analysis is devoted to analyzing the different assemblies where  $\text{Ha}\cdots\text{Ha}$  contacts have a structure directing role. Figure 2a shows a partial view of the X-ray structure of compound **3** showing the formation of infinite 1D assemblies where multiple  $\text{I}\cdots\text{I}$  and  $\text{I}\cdots\text{Br}$  interactions are established. Some distances are similar or shorter than the sum of the corresponding van der Waals radii (contacts marked using black dashed lines) and others are longer (red dashed lines) suggesting weaker contacts. All of them are revealed by the QTAIM analysis of bond critical points (CPs) and bond paths by means of the corresponding bond CP and bond path interconnecting the halogen atoms. We focused the study on a trimeric assembly extracted from the solid state where three HaBs ( $d \leq \Sigma R_{\text{vdw}}$ ) are established (triangle marked in light blue in Figure 2a). The formation energy of the trimer at the PB86-D3/def2-TZVP level of theory is  $-13.8$  kcal/mol, confirming the relevance of this combination of HaB interactions. The QTAIM plots combined with the MEP surface representations is very convenient to differentiate the electron donor and electron acceptor ( $\sigma$ -hole donors) atoms. For the  $\text{I}\cdots\text{Br}$  HaB denoted as “a”, it is quite clear that the bond path crosses the bromines  $\sigma$ -hole (see Figure 2b) and that the negative belt of iodine acts as electron bond donor (see Figure 2c). For the other  $\text{I}\cdots\text{Br}$  contact (denoted as “b”), the bond path crosses the white MEP regions (MEP is close to zero) of both the I and Br atoms (see Figure 2a,c), consequently this contact cannot be considered as a genuine HaB taking into consideration the IUPAC’s definition of HaB. Agreeably, this  $\text{I}\cdots\text{Br}$  contact is significantly longer ( $4.01 \text{ \AA}$ ) than the HaB one ( $3.67 \text{ \AA}$ , see Figure 2a). Finally, for the  $\text{I}\cdots\text{I}$  contact, the bond path connecting the I-atoms crosses the sigma-hole of one iodine atom and the white region of the other one (see Figure 2c,d), thus suggesting that this  $\text{I}\cdots\text{I}$  contact could be defined as a weak HaB at most. In fact, we evaluated the strength of each contact by using the potential energy density ( $V_{\text{T}}$ ) predictor at the bond critical points, which has been proposed in the literature [40]. We used the equation  $E = 0.556 \cdot V_{\text{T}}$  to estimate the association energy of each HaB. This equation has been successfully used before in a variety of halogen bonding interactions [41–49]. As a result, the association energy of HaB “a” is  $-1.67$  kcal/mol, HaB “b” is  $-0.78$ , and HaB “c” is  $-0.88$  kcal/mol.

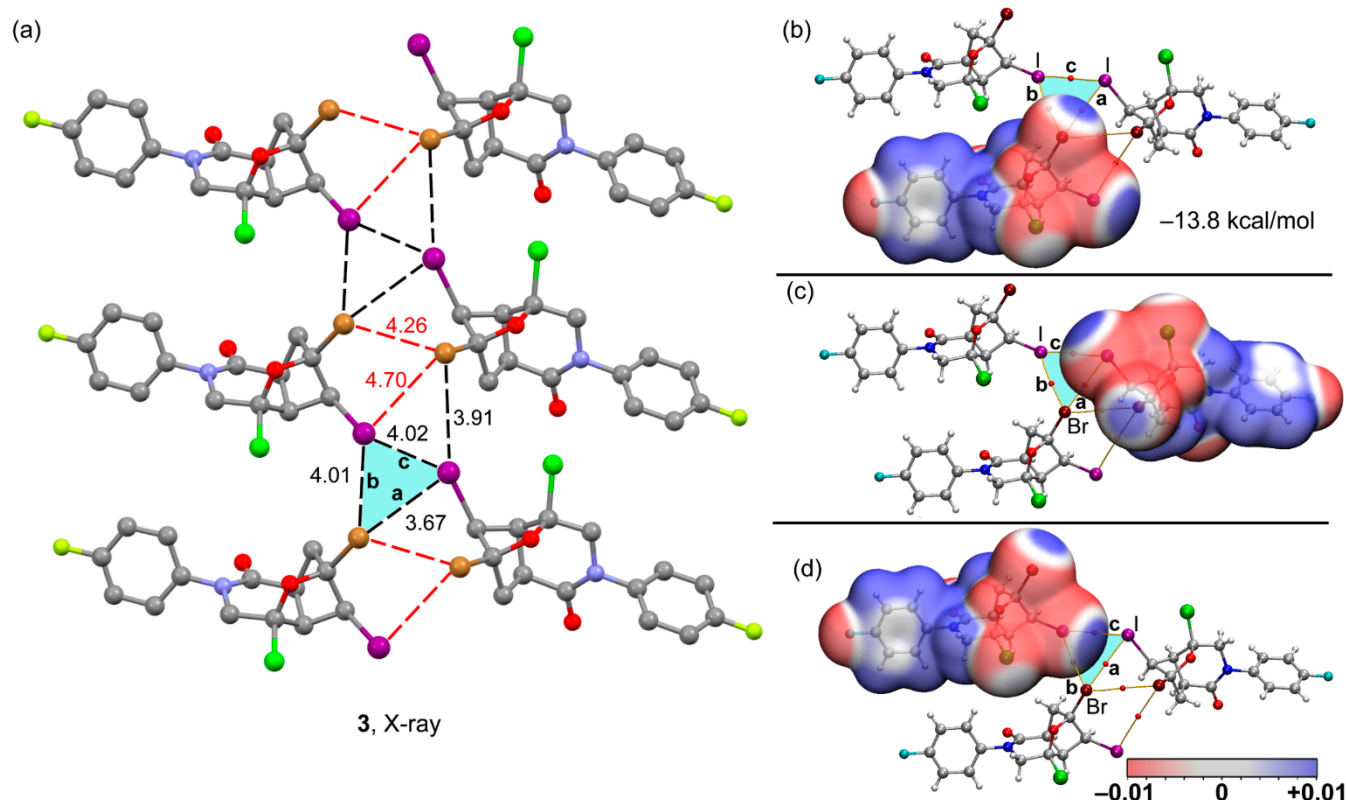


**Figure 2.** (a) Partial view of the X-ray structure of **3**. Distances in Å. (b–d) QTAIM analysis of bond CPs (red spheres) and bond paths (orange lines) of the trimeric assembly of compound **3**. The superimposed MEP surfaces (color scale  $\pm 0.01$  a.u.) are represented.

Similar analysis was performed for compound **4** that also forms supramolecular assemblies in the solid state via multiple  $\text{Ha}\cdots\text{Ha}$  contacts ( $\text{Ha} = \text{Br}$  and  $\text{I}$ ), as depicted in Figure 3a. The contacts marked in black dashed lines present distances that are similar or shorter than  $\Sigma R_{\text{vdw}}$  and those in red correspond to distances much longer than  $\Sigma R_{\text{vdw}}$ . All these contacts are revealed by the QTAIM analysis showing the corresponding bond CPs and bond paths connecting the halogen atoms. We extracted one representative tetramer from the solid state of **4**, to further analyze the  $\text{HaBs}$  denoted as “d” and “e” in Figure 3a, which are important for the formation of the supramolecular assembly. The formation energy is strong ( $-24.8$  kcal/mol) thus validating the structure directing role of such contacts. Figure 3b,c shows the combined MEP/QTAIM plots that confirm the  $\text{HaB}$  nature of both contacts. That is, for the  $\text{I}\cdots\text{Br}$  contact denoted as “d” the bond path crosses the negative belt of Br (Figure 3a) and the  $\sigma$ -hole of I (Figure 3b). In the other  $\text{I}\cdots\text{Br}$  contact (“e”) the bond path crosses through the middle of the Br-atom’s  $\sigma$ -hole (see Figure 3b) and the negative belt of the I-atom (see Figure 3c). It is expected that the  $\text{I}(\sigma\text{-hole})\cdots\text{Br}(\text{LP})$  combination is stronger than the  $\text{Br}(\sigma\text{-hole})\cdots\text{I}(\text{LP})$  one since the former presents the best combination (more positive  $\sigma$ -hole and more negative belt). This agrees well with the longer distance of contact “e” and also the energy of this contact estimated using the  $V_r$  energy predictor that is  $-0.76$  kcal/mol, weaker than contact “d” ( $-1.26$  kcal/mol).

To get further support to the type of halogen bonding interaction observed between the heavier halogen atoms in compounds **3** and **4**, we used the electronic localization function (ELF) method combined with the QTAIM analysis, that has been used recently to differentiate chalcogen and pnictogen bonds in stibanyl telluranes [50]. Such analyses were performed for the trimer and tetramer assemblies of **3** and **4**, respectively, commented above. The ELF topographical 2D maps of  $\eta(r)$  function for the molecular planes defined by the regions in blue in Figures 2 and 3 are represented in Figure 4. The examination of the localization domains corresponding to the lone pairs and  $\sigma$ -hole regions of compound

**3** (Figure 4, left) reveals that in HaB denoted as “a” the negative belts of I interact with the bromine’s  $\sigma$ -hole. This situation is also observed in the I...I contact denoted as “c”. Finally, the distribution of LP and  $\sigma$ -holes in the Br and I atoms involved in the contact denoted as “b” confirms that this contact cannot be defined as a halogen bond. In compound **4**, the ELF analysis shows an almost perfect Br...I  $\sigma$ -hole interaction in the “e” contact where the iodine’s  $\sigma$ -lump points to the bromine’s  $\sigma$ -hole. In the other contact “d”, it can be observed that the bromine’s  $\sigma$ -lump points to the iodine’s  $\sigma$ -hole, though the directionality is worse.

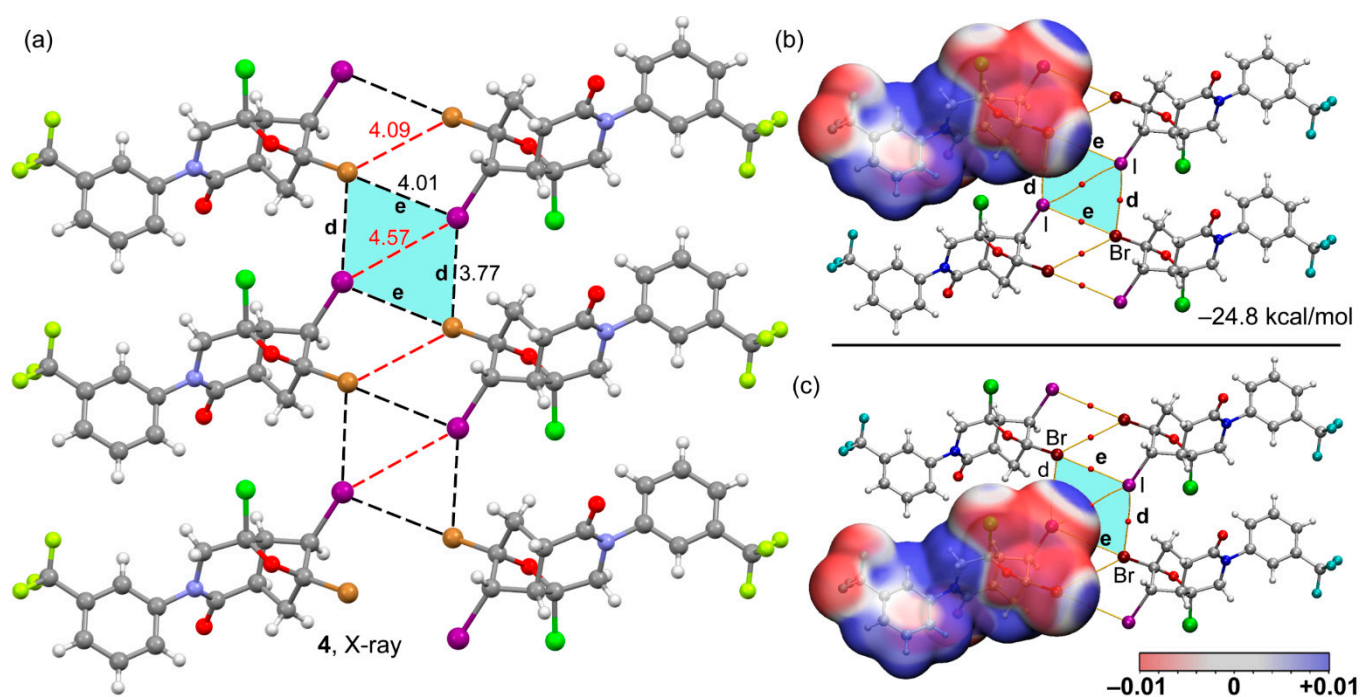


**Figure 3.** (a) Partial view of the X-ray structure of **4**. Distances in Å. (b,c) QTAIM analysis of bond CPs (red spheres) and bond paths (orange lines) of the tetrameric assembly of compound **4**. The superimposed MEP surfaces (color scale  $\pm 0.01$  a.u.) are represented.

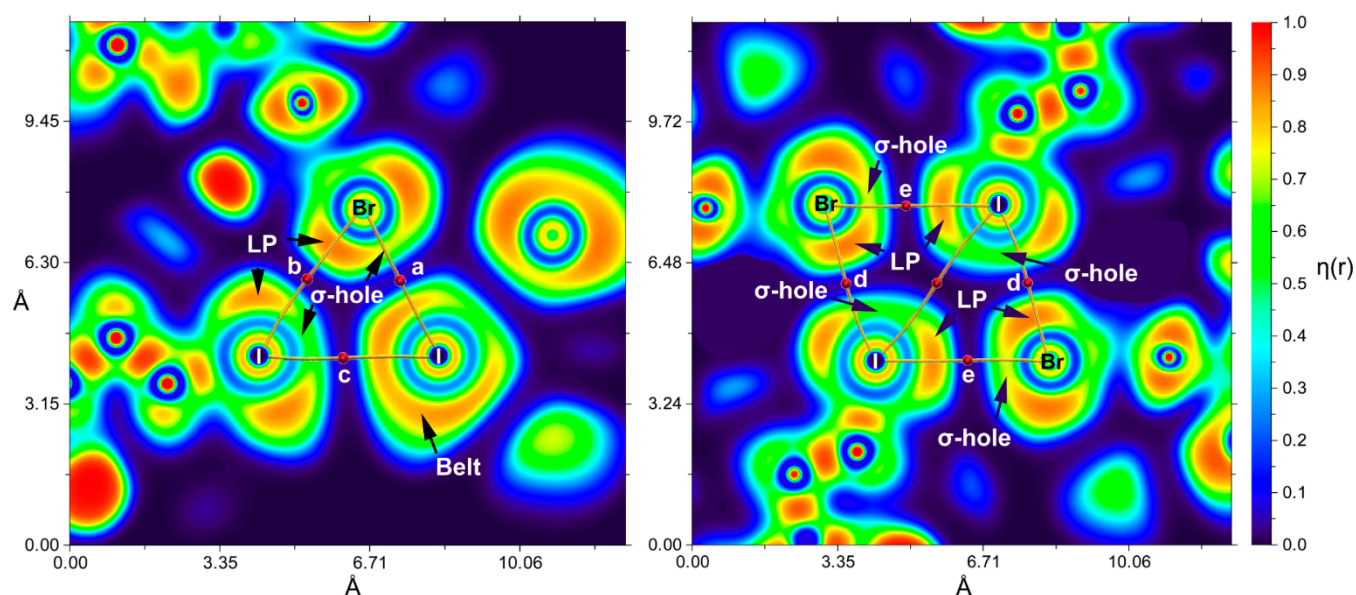


**Figure 4.** 2D maps of  $\eta(r)$  function for the trimer of **3** (left) and tetramer of **4** (right). The molecular planes correspond to the blue regions shown in Figures 2 and 3, respectively.

In general, both QTAIM/MEP and QTAIM/ELF plots are quite informative and useful to differentiate Ha...Ha “like...like” contacts from HaBs. In the former, no clear electron donor and acceptor atoms can be identified and the bond path that connects both atoms crosses the MEP region around the halogen atom where the MEP is negligible (white ring). Therefore, in this type of contact an insignificant contribution of the electrostatic forces is expected, where other terms like polarization or induction effects are dominant.

The analysis of the X-ray structures of compounds **3** and **4** also reveals the existence of additional Br...F (**3**) and Cl...Cl (**3**, **4**) contacts, which have been also analyzed energetically and topologically. Figure 5 (top panel) shows the combined QTAIM and NCIplot analysis of such dimers extracted from the crystallographic coordinates. It can be observed that the contacts are revealed by both topological methods, showing the corresponding bond CPs (red spheres), bond paths, and green isosurfaces connecting the halogen atoms. The QTAIM/MEP plots shown in the lower panel of Figure 5 reveals that only the Br...F contact is a halogen bond where the bond path passes through the bromine's  $\sigma$ -hole. Regarding the Cl...Cl “like...like” contacts in **3** and **4** (Figure 5b,c) the bond paths cross the white regions of the Cl atoms (both dimers are centro-symmetric, so only one MEP surface is shown). The binding energies of the Cl...Cl contacts are  $-0.8$  and  $-1.3$  kcal/mol for compounds **3** and **4**, respectively, thus revealing that these contacts are weak, in line with the green color of the NCIplot isosurface. The interaction energy of the Br...F HaB in **3** is slightly stronger ( $-1.8$  kcal/mol, Figure 5a) likely due to the stronger electrostatic contribution.

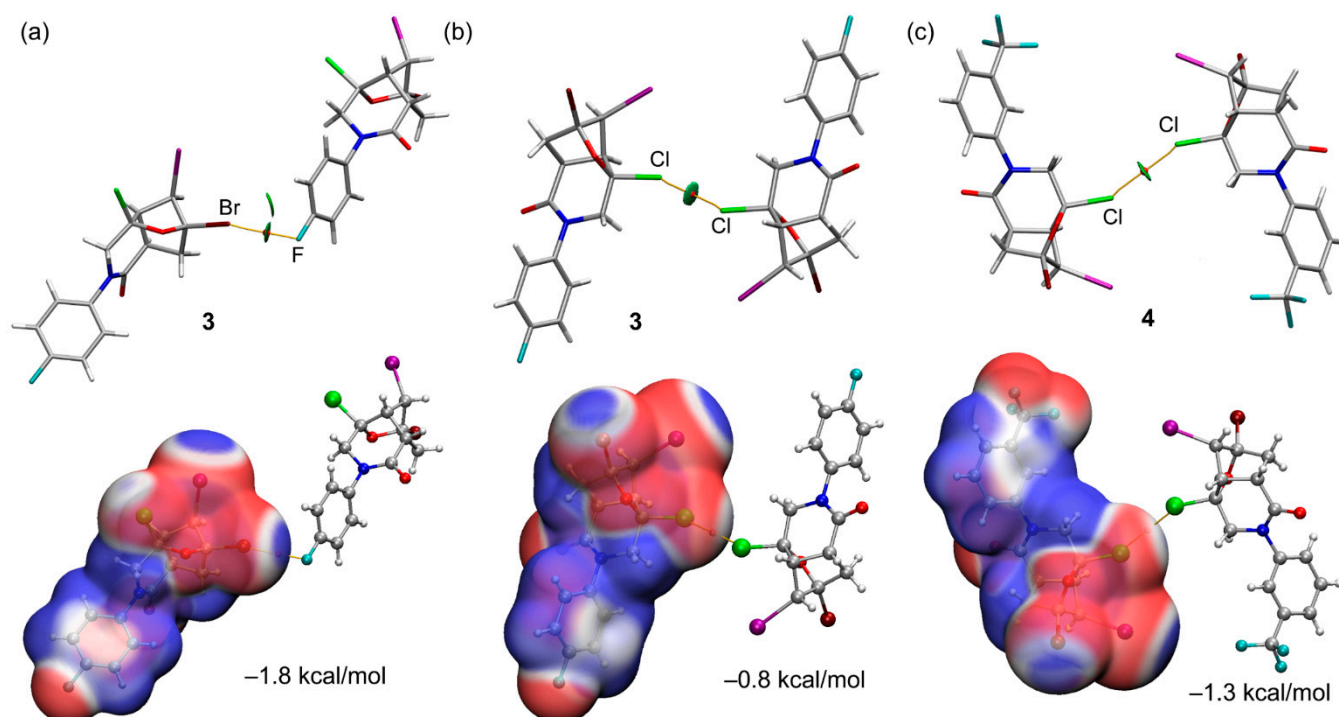


**Figure 5.** Top panel: combined QTAIM (bond CPs in red and bond path as orange lines) and NCIplot (isosurface 0.45) and color range  $-0.04 \text{ a.u.} \leq (\text{sign}\lambda_2)\rho \leq 0.04 \text{ a.u.}$  of the Br...F (a) and Cl...Cl (b) contacts in compound **3** and the Cl...Cl contact (c) in compound **4**. The dimerization energies are also indicated. Level of theory: PB86-D3/def2-TZVP. Lower panel: QTAIM analysis of bond CPs (red spheres) and bond paths (orange lines) of the Ha...Ha dimers where the superimposed MEP surfaces (color scale  $\pm 0.01 \text{ a.u.}$ ) are represented.

#### 4. Conclusions

Two new octahydro-1*H*-4,6-epoxycyclopenta[*c*]pyridin-1-one derivatives that contain the four most abundant halogen atoms (Ha) in their core were synthesized and X-ray characterized. For the synthesis, halogenation was used to initiate the Wagner–Meerwein rearrangement. Both compounds form interesting 1D supramolecular assemblies in the

solid state that propagate by multiple Ha...Ha contacts, that were analyzed using density functional theory (DFT) calculations. We found that the combination of QTAIM/MEP and QTAIM/ELF plots is useful to disclose the nature of these contacts. The strongest Ha...Ha contacts correspond to  $\sigma$ -hole halogen bonds, which range from  $-0.76$  to  $-1.80$  kcal/mol. We expect that the results reported herein would inspire scientists working in the fields of crystal engineering and supramolecular chemistry and the utilization of MEP/QTAIM and MEP/ELF tools to analyze halogen bonds among the theoretical chemistry community.

**Supplementary Materials:** The following are available online at <https://www.mdpi.com/article/10.3390/cryst11111406/s1>, Figure S1:  $^1\text{H}$ ,  $^{13}\text{C}$  and  $^{19}\text{F}$  NMR spectra (in DMSO- $d_6$ ) of **3**, Figure S2:  $^1\text{H}$ ,  $^{13}\text{C}$  and  $^{19}\text{F}$  NMR spectra (in  $\text{CDCl}_3$ ) of **4**, Figure S3: A view of one of two crystallographically independent molecules in **3**. Temperature displacement ellipsoids are shown at 50% probability level, Figure S4: A view of **4**. Temperature displacement ellipsoids are shown at 50% probability level, Figure S5: Packing diagram of **3**, Figure S6: Packing diagram of **4**, Table S1: Fractional Atomic Coordinates ( $\times 10^4$ ) and Equivalent Isotropic Displacement Parameters ( $\text{\AA}^2 \times 10^3$ ) for **3**.  $U_{\text{eq}}$  is defined as 1/3 of the trace of the orthogonalised  $U_{\text{ij}}$  tensor, Table S2: Anisotropic Displacement Parameters ( $\text{\AA}^2 \times 10^3$ ) for **3**. The Anisotropic displacement factor exponent takes the form:  $-2\pi^2[h^2a^2U_{11}+2hka^*b^*U_{12}+\dots]$ , Table S3: Bond Lengths for **3**, Table S4: Bond Angles for **3**, Table S5: Torsion Angles for **3**, Table S6: Hydrogen Atom Coordinates ( $\text{\AA} \times 10^4$ ) and Isotropic Displacement Parameters ( $\text{\AA}^2 \times 10^3$ ) for **3**, Table S7: Fractional Atomic Coordinates ( $\times 10^4$ ) and Equivalent Isotropic Displacement Parameters ( $\text{\AA}^2 \times 10^3$ ) for **4**.  $U_{\text{eq}}$  is defined as 1/3 of the trace of the orthogonalised  $U_{\text{ij}}$  tensor, Table S8: Anisotropic Displacement Parameters ( $\text{\AA}^2 \times 10^3$ ) for **4**. The Anisotropic displacement factor exponent takes the form:  $-2\pi^2[h^2a^2U_{11}+2hka^*b^*U_{12}+\dots]$ , Table S9: Bond Lengths for **4**, Table S10: Bond Angles for **4**, Table S11: Torsion Angles for **4**, Table S12: Hydrogen Atom Coordinates ( $\text{\AA} \times 10^4$ ) and Isotropic Displacement Parameters ( $\text{\AA}^2 \times 10^3$ ) for **4**, Table S13: Atomic Occupancy for **4**.

**Author Contributions:** Conceptualization, R.M.G., F.I.Z. and A.F.; methodology, R.M.G.; validation, R.M.G., F.I.Z. and A.F.; formal analysis, E.V.N., R.M.G. and A.F.; investigation, R.M.G.; resources, A.F.; data curation, D.F.M. and V.P.Z.; writing—original draft preparation, F.I.Z. and A.F.; writing—review and editing, F.I.Z. and A.F.; supervision, F.I.Z. and A.F.; project administration, A.F.; funding acquisition, A.F.; synthesis, D.F.M. and V.P.Z.; X-ray analysis, M.S.G. All authors have read and agreed to the published version of the manuscript.

**Funding:** This paper was prepared with the support of the Russian Foundation for Basic Research (project No 19-03-00807 A) and the MICIU/AEI of Spain (project PID2020-115637GB-I00 FEDER funds).

**Institutional Review Board Statement:** Not applicable.

**Informed Consent Statement:** Not applicable.

**Conflicts of Interest:** The authors declare no conflict of interest.

## References

1. Alkorta, I.; Elguero, J.; Frontera, A. Not Only Hydrogen bonds: Other Noncovalent Interactions. *Crystals* **2020**, *10*, 180. [[CrossRef](#)]
2. Maharramov, A.M.; Mahmudov, K.T.; Kopylovich, M.N.; Pombeiro, A.J.L. (Eds.) *Non-Covalent Interactions in the Synthesis and Design of New Compounds*; John Wiley & Sons, Inc.: Hoboken, NJ, USA, 2016.
3. Davis, H.J.; Phipps, R.J. Harnessing non-covalent interactions to exert control over regioselectivity and site-selectivity in catalytic reactions. *Chem. Sci.* **2017**, *8*, 864–877. [[CrossRef](#)] [[PubMed](#)]
4. Li, Z.T.; Wu, L.Z. (Eds.) *Hydrogen Bonded Supramolecular Structures*; Springer: Berlin/Heidelberg, Germany, 2015.
5. Desiraju, G.R. Supramolecular Synthons in Crystal Engineering—A New Organic Synthesis. *Angew. Chem. Int. Ed.* **1995**, *34*, 2311–2327. [[CrossRef](#)]
6. Metrangolo, P.; Resnati, G. *Halogen Bonding: Fundamentals and Applications (Structure and Bonding)*; Springer: Berlin/Heidelberg, Germany, 2010.
7. Cavallo, G.; Metrangolo, P.; Milani, R.; Pilati, T.; Priimagi, A.; Resnati, G.; Terraneo, G. The Halogen Bond. *Chem. Rev.* **2016**, *116*, 2478–2601. [[CrossRef](#)]
8. Benito, M.; Roselló, Y.; Barceló-Oliver, M.; Frontera, A.; Molins, E. Uracil Derivatives for Halogen-Bonded Cocrystals. *Int. J. Mol. Sci.* **2021**, *22*, 10663. [[CrossRef](#)] [[PubMed](#)]

9. Heinen, F.; Reinhard, D.L.; Engelage, E.; Huber, S.M. A Bidentate Iodine(III)-Based Halogen-Bond Donor as a Powerful Organocatalyst. *Angew. Chem. Int. Ed.* **2021**, *60*, 5069–5073. [[CrossRef](#)]
10. Bulfield, D.; Huber, S.M. Halogen Bonding in Organic Synthesis and Organocatalysis. *Chem. Eur. J.* **2016**, *22*, 14434–14450. [[CrossRef](#)]
11. Michalak, M.; Michalak, K.; Urbanczyk-Lipkowska, Z.; Wicha, J. Synthetic studies on dicyclopenta[*a,d*]cyclooctane terpenoids: Construction of the core structure of fusicoccins and ophiobolins on the route involving a Wagner-Meerwein rearrangement. *J. Org. Chem.* **2011**, *76*, 7497–7509. [[CrossRef](#)]
12. Zubkov, F.I.; Zaytsev, V.P.; Nikitina, E.V.; Khrustalev, V.N.; Gozun, S.V.; Boltukhina, E.V.; Varlamov, A.V. Skeletal Wagner-Meerwein rearrangement of perhydro-3a,6;4,5-diepoxyisoindoles. *Tetrahedron* **2011**, *67*, 9148–9163. [[CrossRef](#)]
13. Morzycki, J.W.; Gryszkiewicz, A.; Jastrzebka, I. Some reactions of 16 $\alpha$ ,17 $\alpha$ -oxido-steroids: A study related to the synthesis of the potent anti-tumor Saponin OSW-1 aglycone. *Tetrahedron Lett.* **2000**, *41*, 3751–3754. [[CrossRef](#)]
14. Chen, Z.-M.; Zhang, Q.-W.; Chen, Z.-H.; Li, H.; Tu, Y.-Q.; Zhang, F.-M.; Tian, J.-M. Organocatalytic Asymmetric Halogenation/Semipinacol Rearrangement: Highly Efficient Synthesis of Chiral  $\alpha$ -Oxa-Quaternary  $\beta$ -Haloketones. *J. Am. Chem. Soc.* **2011**, *133*, 8818–8821. [[CrossRef](#)]
15. Li, H.; Zhang, F.-M.; Tu, Y.-Q.; Zhang, Q.-W.; Chen, Z.-M.; Chen, Z.-H.; Li, J. Enantioselective bromination/semipinacol rearrangement for the synthesis of  $\beta$ -bromoketones containing an all- $\alpha$ -carbon quaternary center. *Chem. Sci.* **2011**, *2*, 1839–1841. [[CrossRef](#)]
16. Girdhar, N.K.; Ishar, M.P.S.; Kumar, R.; Singh, R.; Singh, G. Highly efficient Lewis acid catalyzed, one step conversions of 16 $\alpha$ ,17 $\alpha$ -epoxy-3 $\beta$ -hydroxypregn-5-en-20-one to D-homosteroid and  $\Delta^{13}$ -steroids. *Tetrahedron* **2001**, *57*, 7199–7204. [[CrossRef](#)]
17. Zubkov, F.I.; Mertsalov, D.F.; Zaytsev, V.P.; Varlamov, A.V.; Gurbanov, A.V.; Dorovatovskii, P.V.; Timofeeva, T.V.; Khrustalev, V.N.; Mahmudov, K.T. Halogen bonding in Wagner-Meerwein rearrangement products. *J. Mol. Liq.* **2018**, *249*, 949–952. [[CrossRef](#)]
18. Jung, M.E.; Street, L.J. Novel rearrangements of 7-oxanorbornene systems. *Tetrahedron Lett.* **1985**, *26*, 3639–3642. [[CrossRef](#)]
19. Ciganek, E.; Calabrese, J.C.  $\beta$ -IodoKetones by Prevost Reaction of Vinyl Carbinol. *J. Org. Chem.* **1995**, *60*, 4439–4443. [[CrossRef](#)]
20. Zubkov, F.I.; Nikitina, E.V.; Turchin, K.F.; Aleksandrov, G.G.; Safronova, A.A.; Borisov, R.S.; Varlamov, A.V. Wagner-Meerwein Skeletal Rearrangement of 3-Spiroannulated 6,8a-Epoxy- and 6,8a;7,8-Diepoxyisoquinolines (3-Aza-11-oxatricyclo[6.2.1.0<sup>1,6</sup>]undec-9-enes). Isolation and Identification of 5-Aza-2-oxatricyclo[6.2.1.0<sup>3,9</sup>]undec-3-enes. *J. Org. Chem.* **2004**, *69*, 432–438. [[CrossRef](#)]
21. Zaytsev, V.P.; Mertsalov, D.F.; Trunova, A.M.; Khanova, A.V.; Nikitina, E.V.; Sinelshchikova, A.A.; Grigoriev, M.S. Iodine acetate as a mild selective agent for the Wagner-Meerwein rearrangement in 3a,6-epoxyisoindoles. *Chem. Heterocycl. Compd.* **2020**, *56*, 930–935. [[CrossRef](#)]
22. Shellhamer, D.F.; Allen, J.L.; Allen, R.D.; Gleason, D.C.; Schlosser, C.O.N.; Powers, B.J.; Probst, J.W.; Rhodes, M.C.; Ryan, A.J.; Titterington, P.K.; et al. Ionic Reaction of Halogens with Terminal Alkenes: The Effect of Electron-Withdrawing Fluorine Substituents on the Bonding of Halonium Ions. *J. Org. Chem.* **2003**, *68*, 3932–3937. [[CrossRef](#)]
23. Shellhamer, D.F.; Davenport, K.J.; Forberg, H.K.; Herrick, M.P.; Jones, R.N.; Rodriguez, S.J.; Sanabria, S.; Trager, N.N.; Weiss, R.J.; Heasley, V.L.; et al. Rearrangement of 3-Membered 1,1,2-Trifluorobromonium and Iodonium Ions and Comparison of Trifluorochloronium to Fluorocarbenium Ions. *J. Org. Chem.* **2008**, *73*, 4532–4538. [[CrossRef](#)]
24. Fokin, A.A.; Schreiner, P.R.; Berger, R.; Robinson, G.H.; Wei, P.; Campana, C.F. Pseudotetrahedral Polyhalocubanes: Synthesis, Structures, and Parity Violating Energy Differences. *J. Am. Chem. Soc.* **2006**, *128*, 5332–5333. [[CrossRef](#)] [[PubMed](#)]
25. *SAINT-Plus, Version 7.68*; Bruker AXS Inc.: Madison, WI, USA, 2012.
26. Sheldrick, G.M. *SADABS*; Bruker AXS: Madison, WI, USA, 2008.
27. Sheldrick, G.M. Crystal structure refinement with SHELXL. *Acta Crystallogr. Sect. C* **2015**, *71*, 3–8. [[CrossRef](#)] [[PubMed](#)]
28. Dolomanov, O.V.; Bourhis, L.J.; Gildea, R.J.; Howard, J.A.K.; Puschmann, H. OLEX2: A Complete Structure Solution, Refinement and Analysis Program. *J. Appl. Cryst.* **2009**, *42*, 339–341. [[CrossRef](#)]
29. Ahlrichs, R.; Bar, M.; Haser, M.; Horn, H.; Kolmel, C. Electronic structure calculations on workstation computers: The program system turbomole. *Chem. Phys. Lett.* **1989**, *162*, 165–169. [[CrossRef](#)]
30. Grimme, S.; Antony, J.; Ehrlich, S.; Krieg, H. A consistent and accurate ab initio parametrization of density functional dispersion correction (DFT-D) for the 94 elements H-Pu. *J. Chem. Phys.* **2010**, *132*, 154104. [[CrossRef](#)]
31. Weigend, F.; Ahlrichs, R. Balanced basis sets of split valence, triple zeta valence and quadruple zeta valence quality for H to Rn: Design and assessment of accuracy. *Phys. Chem. Chem. Phys.* **2005**, *7*, 3297–3305. [[CrossRef](#)]
32. Weigend, F. Accurate Coulomb-fitting basis sets for H to Rn. *Phys. Chem. Chem. Phys.* **2006**, *8*, 1057–1065. [[CrossRef](#)]
33. Bauzá, A.; Frontera, A. On the importance of halogen-halogen interactions in the solid state of fullerene halides: A combined theoretical and crystallographic study. *Crystals* **2017**, *7*, 191. [[CrossRef](#)]
34. Yogendra, S.; Hennersdorf, F.; Bauza, A.; Frontera, A.; Fischer, R.; Weigand, J.J. Selective and Reversible Fluoride Complexation from Water by a Cyclic Tri(phosphonio)methanide Dication. *Angew. Chem. Int. Ed.* **2017**, *56*, 7907–7911. [[CrossRef](#)]
35. Bader, R.F.W. A quantum theory of molecular structure and its applications. *Chem. Rev.* **1991**, *91*, 893–928. [[CrossRef](#)]
36. Contreras-García, J.; Johnson, E.R.; Keinan, S.; Chaudret, R.; Piquemal, J.-P.; Beratan, D.N.; Yang, W. NCIPLOT: A program for plotting non-covalent interaction regions. *J. Chem. Theory Comput.* **2011**, *7*, 625–632. [[CrossRef](#)] [[PubMed](#)]
37. Humphrey, W.; Dalke, A.; Schulten, K. VMD: Visual molecular dynamics. *J. Mol. Graph.* **1996**, *14*, 33–38. [[CrossRef](#)]
38. Becke, A.D.; Edgecombe, K.E. A simple measure of electron localization in atomic and molecular systems. *J. Chem. Phys.* **1990**, *92*, 5397. [[CrossRef](#)]

39. Lu, T.; Chen, F. Multiwfn: A multifunctional wavefunction analyzer. *J. Comput. Chem.* **2012**, *33*, 580–592. [[CrossRef](#)] [[PubMed](#)]
40. Zelenkov, L.E.; Ivanov, D.M.; Sadykov, E.K.; Bokach, N.A.; Galmes, B.; Frontera, A.; Kukushkin, V.Y. Semicoordination Bond Breaking and Halogen Bond Making Change the Supramolecular Architecture of Metal-Containing Aggregates. *Cryst. Growth Des.* **2020**, *20*, 6956–6965. [[CrossRef](#)]
41. Torubaev, Y.; Skabitsky, I.V.; Rozhkov, A.V.; Galmes, B.; Frontera, A.; Kukushkin, V.Y. Highly Polar Stacking Interactions Wrap Inorganics in Organics: Lone-pair- $\pi$ -Hole Interactions between the PdO<sub>4</sub> Core and Electron- $\pi$  deficient Arenes. *Inorg. Chem. Front.* **2021**. [[CrossRef](#)]
42. Suslonov, V.V.; Soldatova, N.S.; Ivanov, D.M.; Galmes, B.; Frontera, A.; Resnati, G.; Postnikov, P.S.; Kukushkin, V.Y.; Bokach, N.A. Diaryliodonium Tetrachloroplatinates(II): Recognition of a Trifurcated Metal-Involving  $\mu_3$ -I $\cdots$ (Cl, Cl, Pt) Halogen Bond. *Cryst. Growth Des.* **2021**, *21*, 5360–5372. [[CrossRef](#)]
43. Rozhkov, A.V.; Ananyev, I.V.; Petrov, A.A.; Galmes, B.; Frontera, A.; Bokach, N.A.; Kukushkin, V.Y. Ligand Steric Hindrances Switch Bridging ( $\mu_2$ -I) $\cdots$ O,O to Two-Center I $\cdots$ O Halogen-Bonding Mode in the Assembly of Diketonate Copper(II) Species. *Cryst. Growth Des.* **2021**, *21*, 4073–4082. [[CrossRef](#)]
44. Baykov, S.V.; Geyl, K.K.; Ivanov, D.M.; Gomila, R.M.; Frontera, A.; Kukushkin, V.Y. Azine Steric Hindrances Switch Halogen Bonding to N-Arylation upon Interplay with  $\sigma$ -Hole Donating Haloarenenitriles. *Chem. Asian J.* **2021**, *16*, 1445–1455. [[CrossRef](#)]
45. Zelenkov, L.E.; Eliseeva, A.A.; Baykov, S.V.; Suslonov, V.V.; Galmes, B.; Frontera, A.; Kukushkin, V.Y.; Ivanov, D.M.; Bokach, N.A. Electron belt-to- $\sigma$ -hole switch of noncovalently bound iodine(I) atoms in dithiocarbamate metal complexes. *Inorg. Chem. Front.* **2021**, *8*, 2505–2517. [[CrossRef](#)]
46. Eliseeva, A.A.; Ivanov, D.M.; Rozhkov, A.V.; Ananyev, I.V.; Frontera, A.; Kukushkin, V.Y. Bifurcated Halogen Bonding Involving Two Rhodium(I) Centers as an Integrated  $\sigma$ -Hole Acceptor. *JACS Au* **2021**, *1*, 354–361. [[CrossRef](#)]
47. Efimenko, Z.M.; Eliseeva, A.A.; Ivanov, D.M.; Galmes, B.; Frontera, A.; Bokach, N.A.; Kukushkin, V.Y. Bifurcated  $\mu_2$ -I $\cdots$ (N,O) Halogen Bonding: The Case of (Nitrosoguanidinate)Ni(II) Cocrystals with Iodine(I)-Based  $\sigma$ -Hole Donors. *Cryst. Growth Des.* **2021**, *21*, 588–596. [[CrossRef](#)]
48. Soldatova, N.S.; Postnikov, P.S.; Suslonov, V.V.; Kissler, T.Y.; Ivanov, D.M.; Yusubov, M.S.; Galmes, B.; Frontera, A.; Kukushkin, V.Y. Diaryliodonium as a double  $\sigma$ -hole donor: The dichotomy of thiocyanate halogen bonding provides divergent solid state arylation by diaryliodonium cations. *Org. Chem. Front.* **2020**, *7*, 2230–2242. [[CrossRef](#)]
49. Katlenok, E.A.; Haukka, M.; Levin, O.V.; Frontera, A.; Kukushkin, V.Y. Supramolecular Assembly of Metal Complexes by (Aryl)I $\cdots$ dz2 [Pt(II)] Halogen Bonds. *Chem. Eur. J.* **2020**, *26*, 7692–7701. [[CrossRef](#)]
50. Gomila, R.M.; Frontera, A. Metalloid Chalcogen–pnictogen  $\sigma$ -hole bonding competition in stibanyl telluranes. *J. Organomet. Chem.* **2021**, *954–955*, 122092. [[CrossRef](#)]